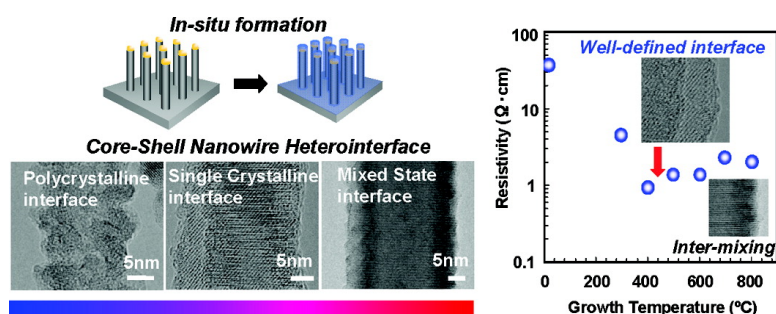**Article**

Effect of the Heterointerface on Transport Properties of in Situ Formed MgO/Titanate Heterostructured Nanowires

Kazuki Nagashima, Takeshi Yanagida, Hidekazu Tanaka,
Shu Seki, Akinori Saeki, Seiichi Tagawa, and Tomoji Kawai

More About This Article

Additional resources and features associated with this article are available within the HTML version:

- Supporting Information
- Links to the 3 articles that cite this article, as of the time of this article download
- Access to high resolution figures
- Links to articles and content related to this article
- Copyright permission to reproduce figures and/or text from this article

View the Full Text HTML

Effect of the Heterointerface on Transport Properties of in Situ Formed MgO/Titanate Heterostructured Nanowires

Kazuki Nagashima, Takeshi Yanagida,* Hidekazu Tanaka, Shu Seki, Akinori Saeki,
Seiichi Tagawa, and Tomoji Kawai

*Institute of Scientific and Industrial Research, Osaka University, 8-1 Mihogaoka, Ibaraki,
Osaka 567-0047, Japan*

Received January 16, 2008; E-mail: yanagi32@sanken.osaka-u.ac.jp

Abstract: Heterostructured transition metal oxide nanowires are potential candidates to incorporate rich functionalities into nanowire-based devices. Although the oxide heterointerface plays a crucial role in determining the physical properties, the effects of the heterointerface on the oxide nanowire's properties have not been clarified. Here we investigate for the first time the significant role of the heterointerface in determining the transport properties of well-defined MgO/titanate heterostructured nanowires by combining a technique for in situ formation of a oxide heterointerface and microwave conductivity measurement. Variation of the heterointerface strongly affects the nanowire's transport properties due to the crystallinity and the atomic interdiffusion at the oxide heterointerface. Thus, the precise in situ formation of a well-defined heterointerface is crucial to create oxide heterostructured nanowires with the desired transport properties.

Introduction

Transition metal oxide nanowires are potential candidates to incorporate desirable physical properties, including superconductivity, ferromagnetism, and ferroelectricity, into nanowire-based devices.[1–4] Since such fascinating oxide materials typically have multiple components,[1–4] one-dimensional nanostructures composed of such multicomponent oxides are highly desired. However, there is a fundamental limitation to fabricating nanowires of various transition metal oxides, resulting from one-dimensional crystal growth mechanisms, such as the vapor–liquid–solid (VLS) mechanism.[5] One of the ways to overcome this critical issue is to utilize a core/shell heterostructured oxide nanowire,[6–8] which allows us to explore a wide range of oxide materials. In oxide heterostructures, the heterointerface is well known to play a crucial role in determining the physical properties.[9–11] Thus, fabricating well-defined heterointerfaces in core/shell heterostructured nanowires is also strongly desir-

able. In situ formation of core/shell heterostructured nanowires would be a powerful method to prevent atmospheric exposure. However, such in situ formation of core/shell heterostructured oxide nanowires, systematic control of the growth, and the effect of the formed heterointerface on the transport properties have not been reported so far. Previously, we have demonstrated the feasibility and the controllability of magnesium oxide (MgO) nanowires formed by using pulsed laser deposition (PLD).[12–15] This in principle allows us to form in situ core/shell heterostructured oxide nanowires. Titanate is a highly attractive material for diverse applications, including uses in photocatalysts,[16] oxide electronics,[17] and nonvolatile memory devices.[18] Here we investigate the in situ formation of MgO/titanate heterostructured oxide nanowires and the effect of the heterointerface on the transport properties. Our results demonstrate the significant role of the heterointerface variation on the

(1) Ramadan, W.; Ogale, S. B.; Dhar, S.; Fu, L. F.; Shinde, S. R.; Kundaliya, D. C.; Rao, M. S. R.; Browning, N. D.; Venkatesan, T. *Phys. Rev. B* **2005**, *72*, 205333.

(2) Takaobushi, J.; Tanaka, H.; Kawai, T.; Ueda, S.; Kim, J. -J.; Kobata, M.; Ikenaga, E.; Yabashi, M.; Kobayashi, K. *Appl. Phys. Lett.* **2006**, *89*, 242507.

(3) Ishikawa, M.; Tanaka, H.; Kawai, T. *Appl. Phys. Lett.* **2005**, *86*, 222504.

(4) Eerenstein, W.; Wiora, M.; Prieto, J. L.; Scott, J. F.; Mathur, N. D. *Nat. Mater.* **2007**, *6*, 348–351.

(5) Hu, J.; Odom, T. W.; Lieber, C. M. *Acc. Chem. Res.* **1999**, *32*, 435–445.

(6) Han, S.; Li, C.; Liu, Z.; Lei, B.; Zhang, D.; Jin, W.; Liu, X.; Tang, T.; Zhou, C. *Nano Lett.* **2004**, *4*, 1241–1246.

(7) Zhang, D.; Liu, Z.; Han, S.; Li, C.; Lei, B.; Stewart, M. P.; Tour, J. M.; Zhou, C. *Nano Lett.* **2004**, *4*, 2151–2155.

(8) Li, C.; Lei, B.; Luo, Z.; Han, S.; Liu, Z.; Zhang, D.; Zhou, C. *Adv. Mater.* **2005**, *17*, 1548–1553.

(9) Nagashima, K.; Yanagida, T.; Tanaka, H.; Kawai, T. *J. Appl. Phys.* **2006**, *100*, 063714.

(10) Nagashima, K.; Yanagida, T.; Tanaka, H.; Kawai, T. *Phys. Rev. B* **2006**, *74*, 172106.

(11) Nagashima, K.; Yanagida, T.; Tanaka, H.; Kawai, T. *J. Appl. Phys.* **2007**, *101*, 026103.

(12) Nagashima, K.; Yanagida, T.; Tanaka, H.; Kawai, T. *J. Appl. Phys.* **2007**, *101*, 124304.

(13) Nagashima, K.; Yanagida, T.; Tanaka, H.; Kawai, T. *Appl. Phys. Lett.* **2007**, *90*, 233103.

(14) Marcu, A.; Yanagida, T.; Nagashima, K.; Tanaka, H.; Kawai, T. *J. Appl. Phys.* **2007**, *102*, 016102.

(15) Yanagida, T.; Nagashima, K.; Tanaka, H.; Kawai, T. *Appl. Phys. Lett.* **2007**, *91*, 016502.

(16) Pan, F.; Zhang, J.; Zhang, W.; Wang, T.; Cai, C. *Appl. Phys. Lett.* **2007**, *90*, 122114.

(17) Hitosugi, T.; Ueda, A.; Nakao, S.; Yamada, N.; Furubayashi, Y.; Hirose, Y.; Shimada, T.; Hasegawa, T. *Appl. Phys. Lett.* **2007**, *90*, 212106.

(18) Kim, K. M.; Choi, B. J.; Shin, Y. C.; Choi, S.; Hwang, C. S. *Appl. Phys. Lett.* **2007**, *91*, 012907.

transport properties of heterostructured oxide nanowires toward the electronic device applications.

Experimental Section

Fabrication of MgO Core Nanowires. MgO nanowires were grown on MgO (100) single-crystal substrate by the Au catalyst-assisted PLD method.[12–15] Prior to the nanowire growth, a Au thin film was deposited on the 5 mm × 5 mm MgO substrate. The background pressure of the PLD chamber was set to 10^{-5} Pa. An ArF excimer laser (Lamda-Physik COMPex 102, $\lambda = 193$ nm) was used for the laser ablation. The MgO single-crystal substrate was used as a source of Mg species vapor. The laser energy and the repetition rate were set to 40 mJ and 10 Hz, respectively. The distance between the substrate and the target was 30 mm. Oxygen gas was introduced into the chamber at a constant ambient pressure of 10 Pa. Prior to the laser ablation, the Au-coated MgO (100) single-crystal substrate was preheated to 800 °C and kept at that temperature for 10 min. After 180 min of deposition, the samples were cooled to room temperature within 30 min under 10 Pa oxygen pressure.

Titanate Shell Layer Growth. A titanate shell layer was grown on vertical arrayed MgO nanowires. The same system used for MgO nanowire growth was used for the shell layer growth. A TiO_2 pellet was used as the target, which was obtained by milling TiO_2 (99.9% pure) powder for 1 h and then sintering at 1000 °C for 24 h. After sintering, the samples were reground for 3 h and then calcined at 500 °C for 5 h. The repetition rate was set to 3 Hz. The laser energy, substrate-to-target distance, oxygen pressure, and substrate temperature were 5–50 mJ, 30–45 mm, 10^{-3}–10 Pa, and room temperature to 800 °C, respectively. The deposition rate for shell layer growth was ~0.4 Å/min. After the deposition, the samples were cooled to room temperature for 30 min.

Sample Characterizations. To characterize the nanowire morphology, field emission electron microscopy (FESEM, JEOL JSM-6330FT) at an accelerating voltage of 30 kV was used. Prior to the FESEM observation, Pt was deposited on the samples to prevent charging. The thickness of Pt was nearly 5 nm. High-resolution transmission electron microscopy (HRTEM, JEOL JEM-3000F) coupled with energy-dispersive spectroscopy (EDS) was used to evaluate the diameter, crystallinity, local crystal structure, and composition of the fabricated nanowires. Samples for HRTEM were prepared by placing a drop of the sample suspension on a copper microgrid (JEOL 7801-11613). HRTEM measurements were performed at an accelerating voltage of 300 kV.

Microwave Conductivity Measurement. For microwave conductivity measurement, the microwave frequency and power were set at ~9.1 GHz and 3 mW, respectively, so that the motion of charge carriers was no disturbed by the low electric field of the microwave. The absorption of microwave power by the samples was monitored as changes in the reflected microwave from a resonant cavity ($Q \approx 2500$) with the samples and measured as a function of the frequency. All the above experiments were carried out at room temperature. The conductivity ($\Delta\sigma$) of the samples is related to the reflected microwave power at the resonant frequency ($\Delta P_r/P_r$) via

$$\langle\Delta\sigma\rangle = \frac{1}{A}\frac{\Delta P_r}{P_r} \qquad (1)$$

where A is a sensitivity factor. The other details of the apparatus are described elsewhere. The absolute value of conductivity was calibrated relative to the value of a thin film grown epitaxially on the MgO substrate, where carrier density and mobility had been determined by a Hall effect measurement.

Results and Discussion

Figure 1a shows the FESEM image of MgO nanowires grown on a MgO (100) single-crystal substrate. All nanowires were grown epitaxially on the substrate. These nanowires are typically
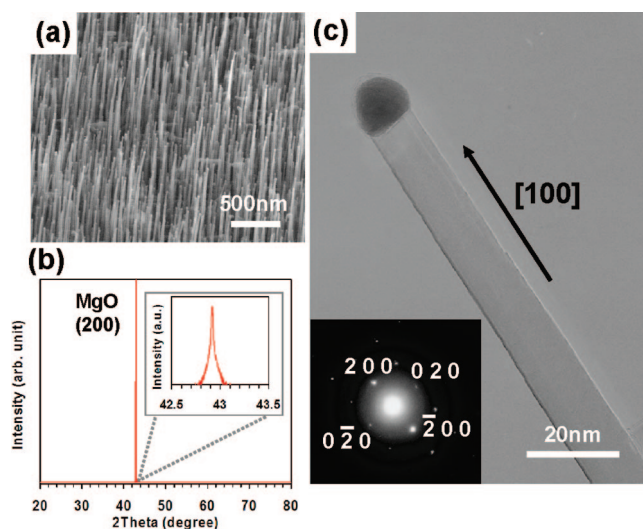

Figure 1. Characteristics of the MgO nanowire template. (a) FESEM image of MgO nanowires grown on MgO (100) substrate. All nanowires were grown epitaxially on the substrate. (b) XRD pattern of MgO nanowires fabricated on MgO (100) single crystal substrate. (c) HRTEM image of an individual MgO nanowire. Inset: SAED pattern of the MgO nanowire, identifying the [100] preferential growth direction.
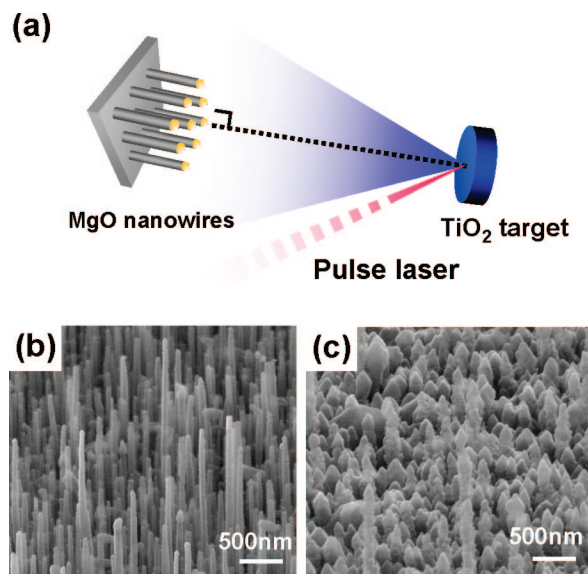

Figure 2. (a) Schematic illustration of the in situ heterostructured nanowire formation using PLD. (b,c) FESEM images of the MgO/titanate heterostructured nanowires grown at laser energies of 15 and 50 mJ, respectively. All heterostructured nanowires were grown at 500 °C and 10^{-3} Pa.

several micrometers long and around 10–20 nm in diameter. X-ray diffraction (XRD) measurement shows only a MgO (200) peak due to the preferential [100] growth of MgO nanowires, as shown in Figure 1b.[12] The preferential crystal growth, single-phase crystallinity, and smooth sidewall were confirmed by HRTEM, as shown in Figure 1c.

A titanate shell layer was deposited on these MgO nanowires by an in situ PLD technique. A schematic of the shell layer formation is illustrated in Figure 2a. Figure 2b,c shows the FESEM images of the MgO/titanate heterostructured nanowires when the ablated particle flux is varied; the nanowires were deposited with laser energies of 15 and 50 mJ, respectively. A clear dependence of the morphologies on the ablated particle flux can be seen. When the laser energy was set to 15 mJ, a
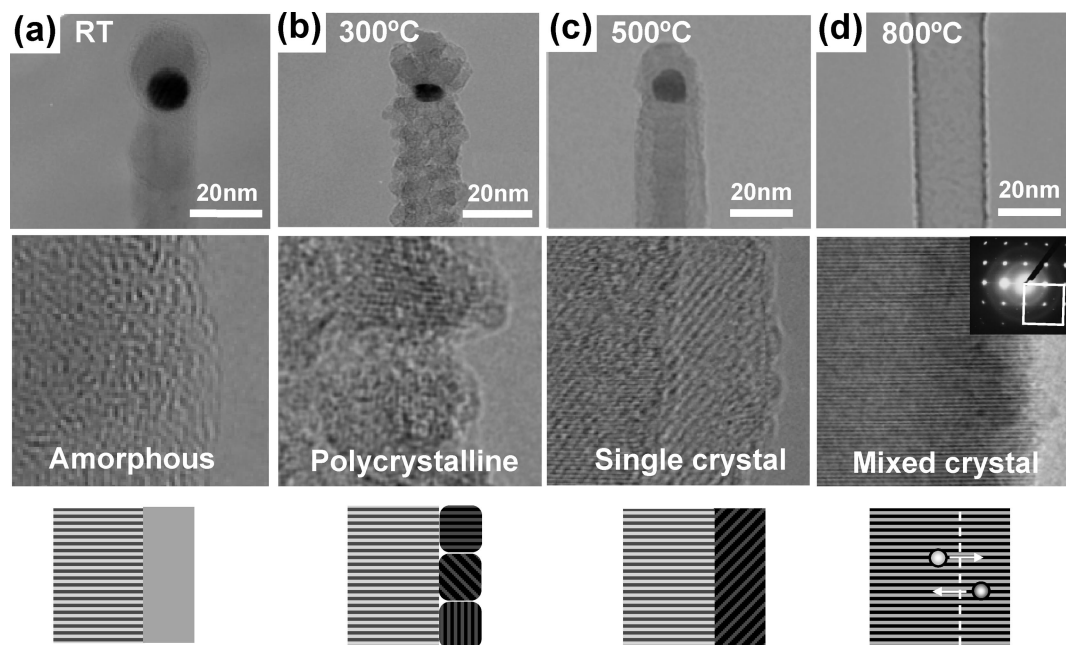
Figure 3. Temperature dependence on the morphologies of MgO/titanate heterostructured nanowires. HRTEM images show the heterostructured nanowires grown at (a) room temperature, (b) 300 °C, (c) 500 °C, and (d) 800 °C. All shell formations were performed at 10^{-3} Pa oxygen pressure and 15 mJ laser energy. The lower figures are magnified images of the heterointerface and schematic illustrations of the heterointerface variations. Inset in (d) is the SAED pattern of nanowires grown at 800 °C.

relatively smooth covering surface was observed, as shown in Figure 2b. Note that shell layers were not observable below a laser energy of 10 mJ due to the absence of adatoms on the surface. On the other hand, a rough surface and grain-like shell layers were found when the laser energy was increased above 20 mJ. In addition, the difference between the bottom diameter and the tip diameter increases with increasing laser energy, indicating the preferential crystal growth and the nucleation on the tip. It is noted that these trends did not depend on the substrate temperature, repetition rate, and deposition time, but strongly depended on both the distance between the target and the substrate and the oxygen pressure, which strongly affect the ablated particle flux. This critical dependence of the nanowire morphologies on ablated particle flux might be due to nucleation phenomena of the ablated species. Generally, when the ablated particle flux is increased, the collision rate between the particles and the probability of nuclear generation increase. Once the nucleus generates at the tip, the ablated particles preferentially assemble the nucleus. As such, the increased ablated particle flux might enhance the preferential growth at the tip, resulting in the large size difference between the tip and the bottom. Thus, controlling the ablated particle flux is crucial to achieve the homogeneous shell covering.

Figure 3 shows the HRTEM images of the MgO/ titanate heterostructured nanowires when the growth temperature was varied from room temperature up to 800 °C at a laser energy of 15 mJ. The core diameter and the shell thickness were typically 10–20 and 5 nm, respectively. Changing the deposition time allows easy control of the shell thickness. There is a wide variation of the heterointerface and the shell layer crystallinity when the temperature is varied. Increasing the growth temperature drastically changes the crystallinity of shell layer from (a) the amorphous phase, (b) the polycrystalline-like structure, (c) the single-crystal core/shell heterostructures, and (d) the mixed crystal structures. The variation from the amorphous phase to the well-defined core/shell heterostructures can be

understood in terms of the enhancement of crystallinity at the heterointerface with increasing temperature. Figure 4a shows the XRD data of nanowires when the growth temperature is varied for the shell layer deposition. It can be seen that the titanate crystallinity changes from the amorphous phase at room temperature to epitaxial (110)-oriented rutile structures at 500 °C. The epitaxial growth is illustrated in Figure 4b. In fact, these trends basically agree with the HRTEM results in Figure 3. Such variation of crystallinity with varying growth temperature was found on titanate thin films grown on MgO (100) substrate (see Figure S1 in the Supporting Information). However, the presence of polycrystalline structure at 300 °C differs from the case of the thin films, since the thin films grown at 300 °C showed the epitaxial growth of mixed (110)-oriented rutile structure and (100)-oriented anatase structure. This discrepancy might be due to the limitation of surface migration on the nanowire sidewall. The presence of (110)-oriented rutile structure was no longer observable when the growth took place at 800 °C, indicating a change of crystal structure. To identify the crystal structures grown at high temperature, fine XRD scans were performed, as shown in Figure 4c. A shoulder-like peak was observed below the MgO (200) peak, and the lattice constant around the peak is consistent with possible $(Mg,Ti)_3O_4$ spinel structures. The selected area electron diffraction (SAED) patterns for nanowires formed at 800 °C agreed with such cubic spinel structures, as shown in Figure 3. This implies Mg diffusion into the shell layers during shell layer formation. In addition, as shown in Figure 4d, the EDS measurement demonstrates that the atomic ratio of Mg/Ti is nearly 1:1, indicating the formation of $Mg_{1.5}Ti_{1.5}O_4$ spinel structure. The Mg diffusion length in this system is over 200 nm (see Figure S2 in the Supporting Information) and large enough compared with the shell thickness of 5 nm. These results clearly indicate that the crystal structure of nanowires formed at 800 °C is a mixed spinel structure.

The above results highlight the wide variation of the heterointerface in oxide nanowires when the ambient atmosphere
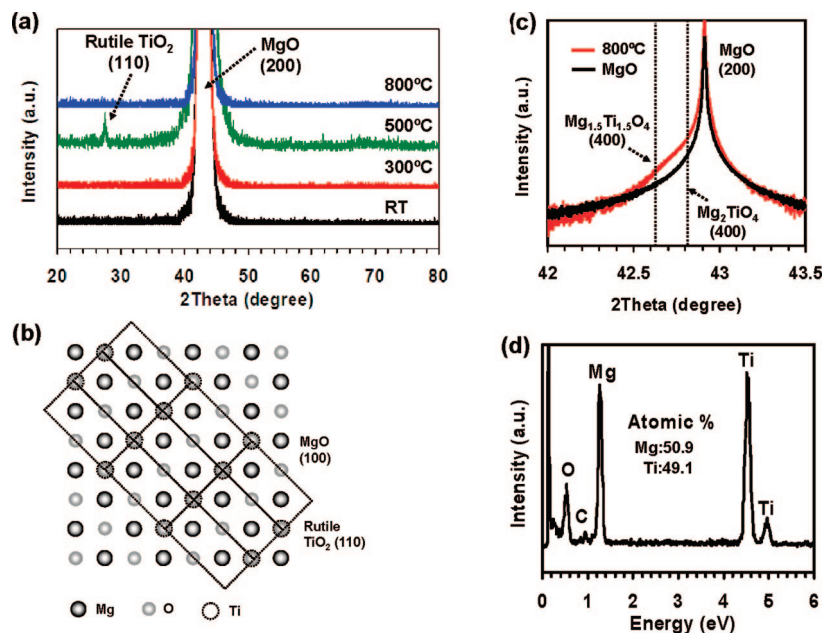
Figure 4. (a) XRD patterns of the MgO/titanate heterostructured nanowires with varying formation temperature. (b) Schematic of the epitaxial growth of rutile TiO_2 on MgO. The TiO_2 (110) plane and the MgO (100) plane match well by the long-range epitaxial rule of 6:13. (c) Fine XRD pattern of MgO/titanate heterostructured nanowires grown at 800 °C. (d) EDS data of the MgO/titanate heterostructured nanowires grown at 800 °C. All shell formations were performed at 10^{-3} Pa oxygen pressure.

is varied. In principle, such heterointerface variation should affect the charge carrier transport properties of heterostructured nanowires. One of critical issues in measuring the transport properties of nanowires is the contact with electrodes at the nanoscale. Microwave conductivity measurement allows us to investigate the transport properties of such nanoscale materials without electrodes and contact problems.[19,20] Figure 5 shows the results of microwave conductivity measurements for heterostructured oxide nanowires when the growth temperature was varied from room temperature up to 800 °C. The microwave conductivity measurements were performed at 300 K.

There are two major trends in the transport when the growth temperature was varied. First, the resistivity decreased when the growth temperature increased below 400 °C. The enhancement of electrical conductivity below 400 °C can be interpreted in terms of the crystal variation from the amorphous phase to the single-crystal core/shell heterostructures, as can be seen in the HRTEM images (Figure 3). Such reduction of resistivity with increasing growth temperature from room temperature to 400 °C was also found in titanate thin-film growth, as shown in Figure 5d (see Figure S3 in the Supporting Information). Thus, the enhancement of crystallinity at the heterointerface is responsible for the observed trend in heterostructured nanowires grown below 400 °C. However, it is noted that the resistivity of nanowires grown at 300 °C is rather high, even in comparison with the trend in the case of thin films. This discrepancy is due to the difference in crystallinity between the nanowires and the thin films. As shown in Figure 3, the heterostructured nanowires showed polycrystalline-like structure, whereas the thin films were grown epitaxially. It should be emphasized that the

resistivity of the heterostructured nanowires grown at 400 °C is comparable to that of the thin films, as shown in Figure 5c. This indicates the high quality of the shell layer in the heterostructured nanowires achieved by controlling appropriately the ambient atmosphere. Thus, the above results highlight that the crystal difference at the heterointerface strongly affects the transport properties of heterostructured nanowires.

Second, above a growth temperature of 400 °C, the resistivity increased through the minimum with increasing growth temperature. This can be understood in terms of the formation of mixed $Mg_{2-x}Ti_{1+x}O_4$ spinel structures at relatively high temperatures, since Mg_2TiO_4 is an insulator.[21] The presence of mixed $Mg_{2-x}Ti_{1+x}O_4$ spinel structures has been discussed (Figure 4). However, the resistivity of heterostructured nanowires grown at 800 °C is rather low when compared with the trends of the thin films (Figure 5d). This would be due to the composition of mixed $Mg_{2-x}Ti_{1+x}O_4$ spinels, because increasing x results in decreasing resistivity.[21] In thin films, Mg atoms can be supplied from single-crystal substrate, whereas there is a limit of Mg atoms for heterostructured nanowires. As shown in Figure 4d, the composition of spinel structure for nanowires formed at 800 °C is $Mg_{1.5}Ti_{1.5}O_4$. As such, the composition difference in mixed spinel structures causes the discrepancy between the transport properties of the heterostructured nanowires and the thin films. Thus, the nature of the mixing at the heterointerface strongly affects the transport properties of MgO/titanate core–shell nanowires. The above results highlight that realizing the desired transport properties in well-defined oxide heterostructured nanowires requires the precise

(19) Yamamoto, Y.; Fukushima, T.; Suna, Y.; Ishii, N.; Saeki, A.; Seki, S.; Tagawa, S.; Taniguchi, M.; Kawai, T.; Aida, T. *Science* **2007**, *314*, 1761–1764.

(20) Hoofman, Romano, J. O. M.; de Haas, Matthijs, P.; Siebbeles, Laurens, D. A.; Warman, John, M. *Nature* **1998**, *392*, 54–56.

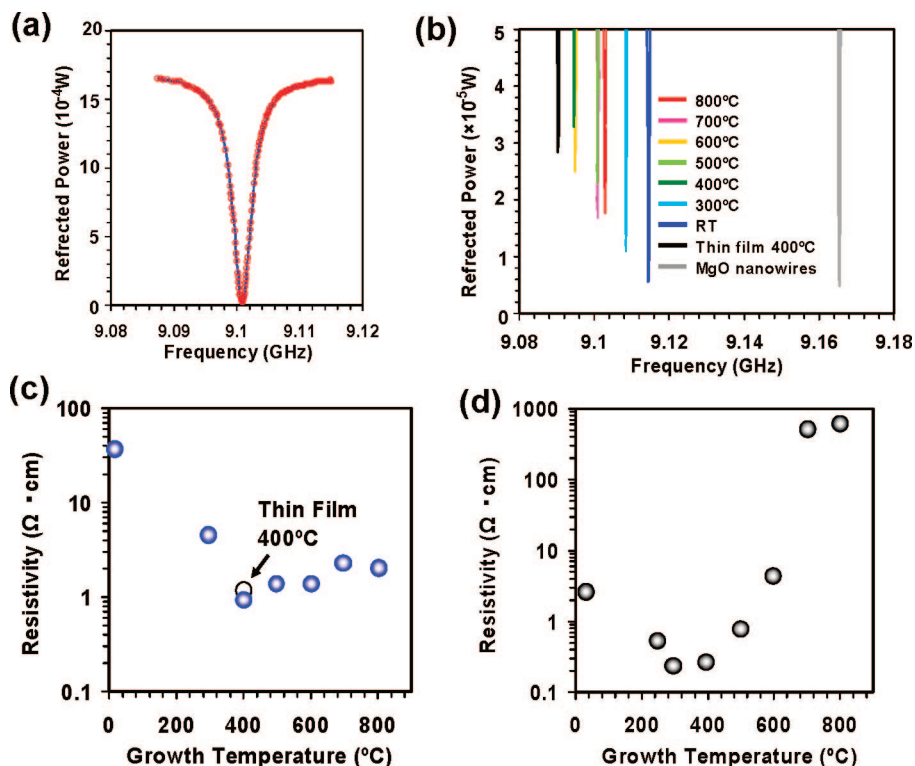(21) Isobe, M.; Ueda, Y. *J. Alloys Compd.* **2004**, *383*, 85–88.

Figure 5. (a,b) Dependence of microwave power, reflected from the cavity of the samples, on the frequency. (a) Entire views of the typical resonance curve in microwave measurement for heterostructured nanowires grown at 500 °C. (b) Magnified views at the resonance frequencies of heterostructured nanowires when the formation temperature was varied. (c,d) Effects of formation temperature on the resistivity of (c) MgO/titanate heterostructured nanowires and (d) thin films, respectively. All shell formations were performed at 10^{-3} Pa oxygen pressure.

control of the crystal formation and the atomic interdiffusion at the oxide heterointerface.

Conclusion

In summary, we investigated the effect of the heterointerface on the transport properties of in situ formed MgO/titanate heterostructured nanowires by using PLD. The in situ formation of the heterointerface was found to be strongly dependent on both the ablated particle flux and the growth temperature. By controlling appropriately the ambient atmosphere during the in situ heterostructure formation, it is possible to fabricate a well-defined oxide heterointerface in nanowires, which is comparable with thin films in terms of the transport properties. In addition, variations in the heterointerface strongly affect the transport properties via the crystallinity and the atomic interdiffusion at the oxide heterointerface. Thus, the precise in situ formation of well-

defined heterointerface is crucial to create the desired transport properties in oxide heterostructured nanowires.

Supporting Information Available: Results of the crystal structures and the transport properties in titanate thin films deposited on MgO (100) substrate with varying deposition conditions, including the substrate temperature and the film thickness. This material is available free of charge via the Internet at http://pubs.acs.org.

JA800367A